Environmental Pollution 335 (2023) 122269

Contents lists available at ScienceDirect

Environmental Pollution

journal homepage: www.elsevier.com/locate/envpol

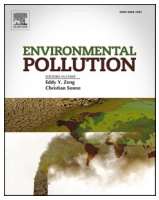

Spatial heterogeneity in global atmospheric CO during the COVID–19 lockdown: Implications for global and regional air quality policies☆

M. Pathak, V.K. Patel, J. Kuttippurath *

CORAL, Indian Institute of Technology Kharagpur, Kharagpur, 721302, India

ARTICLE INFO

Keywords:
COVID–19
Carbon monoxide
Lockdown
Air quality
Troposphere
Anthropogenic

ABSTRACT

The COVID–19 lockdown (LD) provided a unique opportunity to examine the changes in regional and global air quality. Changes in the atmospheric carbon monoxide (CO) during LD warrant a thorough analysis as CO is a major air pollutant that affects human health, ecosystem and climate. Our analysis reveals a decrease of 5–10% in the CO column during LD (April–May 2020) compared to the pre-lockdown (PreLD, March 2020) periods in regions with high anthropogenic activity, such as East China (EC), Indo-Gangetic Plain (IGP), North America, parts of Europe and Russia. However, this reduction did not occur in the regions of frequent and intense wildfires and agricultural waste burning (AWB). We find high heterogeneity in the CO column distributions, from regional to city scales during the LD period. To determine the sources of CO emissions during LD, we examined the ratios of nitrogen dioxide (NO_2), sulfur dioxide (SO_2) to CO for major cities in the world. This facilitated the identification of contributions from different sources; including vehicles, industries and biomass burning during LD. The comparison between CO levels during the LD and PreLD periods indicates a notable reduction in the global tropospheric CO, but no significant change in the stratosphere. It is found that CO emissions decreased during LD in the hotspot regions, but rebounded after the LD restrictions were lifted. This study, therefore, highlights the importance of policy decisions and their implementations in the global and regional scales to improve the air quality, and thus to protect public health and environment.

1. Introduction

Air pollution is currently a serious global problem due to its detrimental effects on the public health and natural environment (WHO, 2022). According to the most recent estimate from WHO (2022), over 99% of world's population is exposed to poor air quality. Carbon Monoxide (CO), a highly reactive gas essential for atmospheric carbon cycle (Novelli et al., 1998), is one of the major air pollutants with high mixing ratio in the troposphere, affects human health, ecosystem and climate (Khalil and Rasmussen, 1990; Chen et al., 2020). CO is emitted primarily from the combustion of fossil fuels and biomass, as well as natural processes such as the oxidation of organic compounds like methane and isoprene. Fossil fuel combustion dominates its concentrations in the northern hemisphere, but biomass burning in the southern hemisphere (Holloway et al., 2000; Buchholz et al., 2018; Zheng et al., 2019). Additionally, all aforesaid activities, but fire activity in the hotspot regions, have increased significantly across the latitudes in the past few decades (Joshi et al., 2023). Strict regulations on the anthropogenic activities may have a high impact on the air quality by reducing emissions. This can be observed from the COVID–19 lockdown (LD), where improvement in air quality is found in many countries due to strict restriction on anthropogenic activities.

The COVID-19 (Coronavirus, 2019 or SARS-CoV-2) pandemic started in December 2019, which posed a global threat to human lives. Governments worldwide implemented stringent measures to contain the spread of the virus, including restrictions on public movement and activities. The COVID-19 situation made a unique opportunity to examine how the large-scale and rapid reductions in emissions can lead to changes in regional and global air quality. By conducting the global-scale analysis, we can acquire crucial information about how the human-induced abrupt decrease in emissions propelled modifications in air pollution.

Several studies have documented reductions in emissions during the COVID-19 lockdown. For instance, Guevara et al. (2021) estimated the reduction in electricity consumption, road traffic and aviation emissions in Europe. Lapatinas (2020) found that restrictive measures during the

☆ This paper has been recommended for acceptance by Da Chen.

* Corresponding author.
E-mail address: jayan@coral.iitkgp.ac.in (J. Kuttippurath).

https://doi.org/10.1016/j.envpol.2023.122269
Received 31 May 2023; Received in revised form 20 July 2023; Accepted 25 July 2023
Available online 29 July 2023

partial and full LD reduced mobility across Europe. Hammam et al. (2022) observed a significant reduction in the concentration of NO_2 (– 44.5%), CO (– 41.5%) and $PM_{2.5}$, PM_{10} (– 29.5%, each) in Jeddah (Saudi Arabia) during the LD period as compared to those in the pre-lockdown (PreLD). Majority of studies on air quality changes during LD focused on a single city, country, air pollutant or region (e.g., Krecl et al., 2020; Singh et al., 2020; El-Sheekh and Hassan (2021); Grange et al., 2021; Shi et al., 2021; Said et al., 2022). Sokhi et al. (2021) found significant decrease in CO concentration during LD across the Chinese, Indian, American and European cities. Similarly, Bhat et al. (2021) reported reduction in CO in many global cities during LD. Bray et al. (2021) identified changes in the global air quality during LD compared to that averaged for the period of 2015–2019 using satellite observations, which showed a decline in the CO concentrations (4% below average) in India, China, and the USA during LD. Most studies deal with changes in the air quality during LD compared to previous years, and only a few have examined changes after the restrictions were lifted. Therefore, a dedicated study in different spatial scales is needed to demonstrate changes in the global air quality during LD in comparison to PreLD and post-lockdown (PostLD) periods.

We investigate the changes in global CO levels from surface to stratosphere for the LD period to know the impact of changes in human activities on the air quality, as CO is one of the major air pollutants. This will give us a better understanding of the policy decisions needed to cope with the dynamic air pollution episodes across the hotspots, cities, small towns and other regions. We utilize the CO observations from Atmospheric Infrared Sounder (AIRS), Measurement of Pollution in The Troposphere (MOPITT), Modern-Era Retrospective analysis for Research and Applications (MERRA–2), and TROPOspheric Monitoring Instrument (TROPOMI) to understand the global changes in CO during three distinct periods. We also conduct the regional analyses, by examining the changes in CO hotspot regions such as Central Africa (CA), Central Asia (CEA), Southeast Asia (SEA) and South America (SA). Additionally, we analyse the changes in CO across the countries and 3000 cities worldwide. The policy implications of reduced CO in the global and regional scales in relation to the environmental changes during the LD period are also assessed.

2. Data and methods

2.1. Study area and selection of regions

Other than the global changes in CO, we have also considered some specific regions for our analysis, and are shown in Fig. 1 and Figure S1. For example, CA, CEA, SEA and SA, which are the global hotspots of CO. These regions are selected based on the sources of CO that vary from

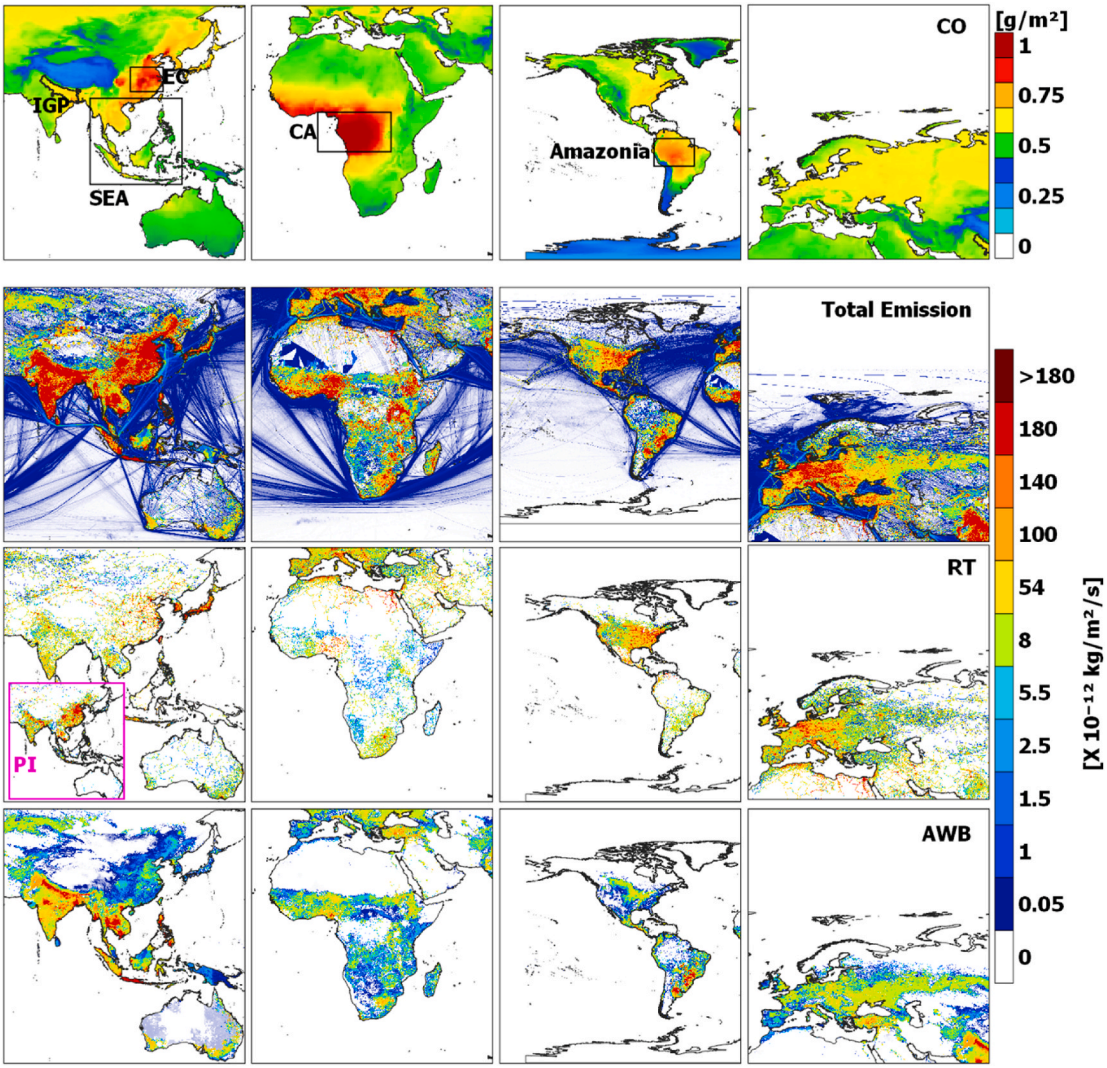

Fig. 1. Distribution of CO column from MERRA-2 (top panel) and emissions from different sectors such as road transport (RT), power industry (PI) and agriculture waste burning (AWB) taken from EDGARv6.1 inventory for the period of 2010–2018. Hotspot regions are also marked, such as East China (EC), Indo-Gangetic Plain (IGP), Southeast Asia (SEA), Central Africa (CA) and Amazonia.

biomass burning to industrial emissions. For instance, SA and CA have CO emissions mostly from the biomass burning, whereas both industrial and biomass burning are the sources of CO in SEA. Furthermore, to understand the changes in CO in small spatial scales, where LD is more effective, globally 3000 cities with population more than 50000 are selected, which cover regions in all six continents. These cities are representative of the regions with different climatic, environmental and socioeconomic conditions. Even though these are some of the most important urban centers in the world, the scales in which they operate (geographically, population-wise and in terms of environment) are quite different, ranging from megacities to small towns. We have also considered 4 distinct regions in Russia, North America (NA), SA and South Africa, far away from cities and anthropogenic sources of NO_2, CO and SO_2, to further examine the changes in air pollution during LD.

2.2. Definition of the LD period

To define the PreLD, LD and PostLD periods, we investigated the LD period of all nations and validated with auxiliary data sources and studies (Sokhi et al., 2021). For a comprehensive global analysis, we considered a common time period for LD, when most cities were under strict regulations on movement. This information is used for defining the stages of LD, and ensured a comparable standard to be applied within and between cities and regions for the analysis. A small number of cities did not strictly adhere to the definition of LD, because the measures to restrict the movement, and activities of people were depending on the rapidly evolving national and local responses to the pandemic. Here, the periods are defined as LD (April–May), PreLD (March) and PostLD (June–September) in the year 2020. PreLD period is defined as the period before the complete restriction on mobility were imposed by the government authorities. Similarly, LD means the full restriction on movement and other anthropogenic activities. The period after LD is referred to as PostLD, during which partial or complete relaxation is permitted for movement and socio-economic activities.

2.3. The CO, NO_2 and SO_2 data

AIRS introduced the grating spectrometer onboard the AQUA spacecraft that launched in 2002. The instrument has 2378 channels and can record the intensity of outgoing thermal radiation at 3.74–4.61 μm (2169–2674 cm^{-1}), 6.20–8.22 μm (1217–1613 cm^{-1}), 8.8–15.4 μm (649–1136 cm^{-1}), with a spectral resolution ($\lambda/\Delta\lambda$) of 1200 (Aumann et al., 2003; Filonchyk et al., 2020). Here, the monthly mean CO mixing ratio from surface to stratosphere is taken for the years from 2017 to 2021. In addition, the total column CO obtained from the MOPPIT instrument for the period 2017–2021 at a spatial resolution of $1^\circ \times 1^\circ$ is also considered. MOPITT is an instrument onboard the Earth Observing System Terra spacecraft and its primary objective is to measure the tropospheric column of global CO. The measurements obtained from MOPITT allow investigation of the distribution, transport, sources and sinks of CO (Joshi et al., 2023).

Among the products of atmospheric reanalysis, MERRA–2 is one of the most recent and widely used (Gelaro et al., 2017). It is an improved version of the MERRA dataset. Using observations from a variety of satellites, the global total column mass density of CO has also been assimilated into MERRA–2. Here, the total column CO from MERRA-2 is taken for the period 2017–2021, and has a spatial resolution of $0.5^\circ \times 0.625^\circ$.

We have used the NO_2, SO_2 and CO observations from TROPOMI at a resolution of 3.5×5.5 km^2 for the period of 2019–2021 to analyse the changes in small spatial scales (i.e. cities). These total column CO data are retrieved from TROPOMI onboard the Sentinel-5 Precursor satellite, which uses modified shortwave infrared retrieval algorithm based on the CO absorption spectral bands in 2305–2385 nm (Landgraf et al., 2018).

We have analysed the burnt area using OLCI (Ocean and Land Colour Instrument) v 1.1 data at grid scale ($0.25^\circ \times 0.25^\circ$) for the period of 2017–2021 to understand the changes of CO in the biomass burning regions. These data are obtained through the analysis of reflectance changes from the medium resolution sensors (Terra MODIS and Sentinel-3 OLCI), supported by the use of MODIS thermal information. The burned area data also include information related to the land cover that has been burned. There is no direct impact of LD on regions with non-anthropogenic sources, but seasonal variability of burned biomass can be related to the CO column in those areas.

The MOPITT satellite instrument provides the longest observations of CO from space. Buchholz et al. (2017) validated the MOPITT CO observations using the ground-based Fourier transform infrared (FTIR) spectrometers across the latitudes, and found that the former overestimates the latter by about 10%. For the thermal infrared (TIR), the mean bias is 2.4%, but slightly higher, about 5.1% for TIR–NIR (multispectral) and 6.5% for NIR (near infrared). Similarly, the AIRS CO profiles are validated globally by Hegarty et al. (2022) using the ground-based and aircraft measurements, and found a mean bias of $+6.6 \pm 4.6\%$, $+0.6 \pm 3.2\%$, and $-6.1 \pm 3.0\%$ at 750, 510, and 287 hPa altitudes, respectively. The TROPOMI CO retrievals over land show an excellent agreement with that of MOPITT, and the average bias compared to the MOPITT TIR, NIR, and TIR+NIR data is $-3.73\% \pm 11.51\%$, $-2.24\% \pm 12.38\%$, and $-3.22\% \pm 11.13\%$, respectively (Apituley et al., 2018; Martínez-Alonso et al., 2020).

The percentage change in CO is calculated for the LD period with respect to the average CO during 2017–2019 and 2021 for the same months/period corresponding to LD in 2020. Similarly, changes during LD are also computed with respect to PreLD period. This computation is carried out for all selected regions, cities and countries. The effect of LD in regions having sources of CO other than anthropogenic is not examined yet. Therefore, we will be looking into the impact of LD on all major CO sources across the globe. Detailed methodology is given in Supplementary material.

3. Results and discussion

3.1. Major global hotspots and sources of CO

Sources of anthropogenic origin including industries and transport were shut down during LD in 2020, whereas the domestic, AWB and forest fire events were the active sources of CO emissions globally. Therefore, first, it is necessary to understand the general distribution and identify the regions of high CO. Here, we analyse the global distribution of CO along with emissions from all sectors, road transport, power industry and AWB, as shown in Fig. 1. We find that the heterogeneity of CO in the hotspot regions is due to different sources such as biomass burning, industrial, vehicular, residential and AWB. Regions dominated by biomass burning have very high CO emissions. For example, CA (about 1 g/m^2), Amazonia (0.75 g/m^2) and SEA (0.5–0.75 g/m^2) have high CO column. Comparatively high values are also observed in the industrial hubs like East China (EC, 0.75–1 g/m^2), which match well with emission inventory, where the emissions of CO from power industries (140–180 $\times 10^{-12}$ $kg/m^2/s$) are very high. Similarly, CO column is very high in Indo-Gangatic Plain (IGP, 0.75 g/m^2), which is dominated by AWB (100–180 $\times 10^{-12}$ $kg/m^2/s$), residential and industrial emissions. Furthermore, AWB is prominent in SEA (54–180 $\times 10^{-12}$ $kg/m^2/s$), as found from the emission inventory (Fig. 1). Similarly, higher values of CO column in the USA (0.5–0.75 g/m^2) and Western Europe (0.625 g/m^2) are ditected by the emissions from road transport [the USA (54–140 $\times 10^{-12}$ $kg/m^2/s$) and Western Europe (8–180 $\times 10^{-12}$ $kg/m^2/s$)].

3.2. Relative changes in CO during LD compared to PreLD

Fig. 2 illustrates the changes in global CO column using MERRA-2 data during LD compared to PreLD. Most regions show a reduction in

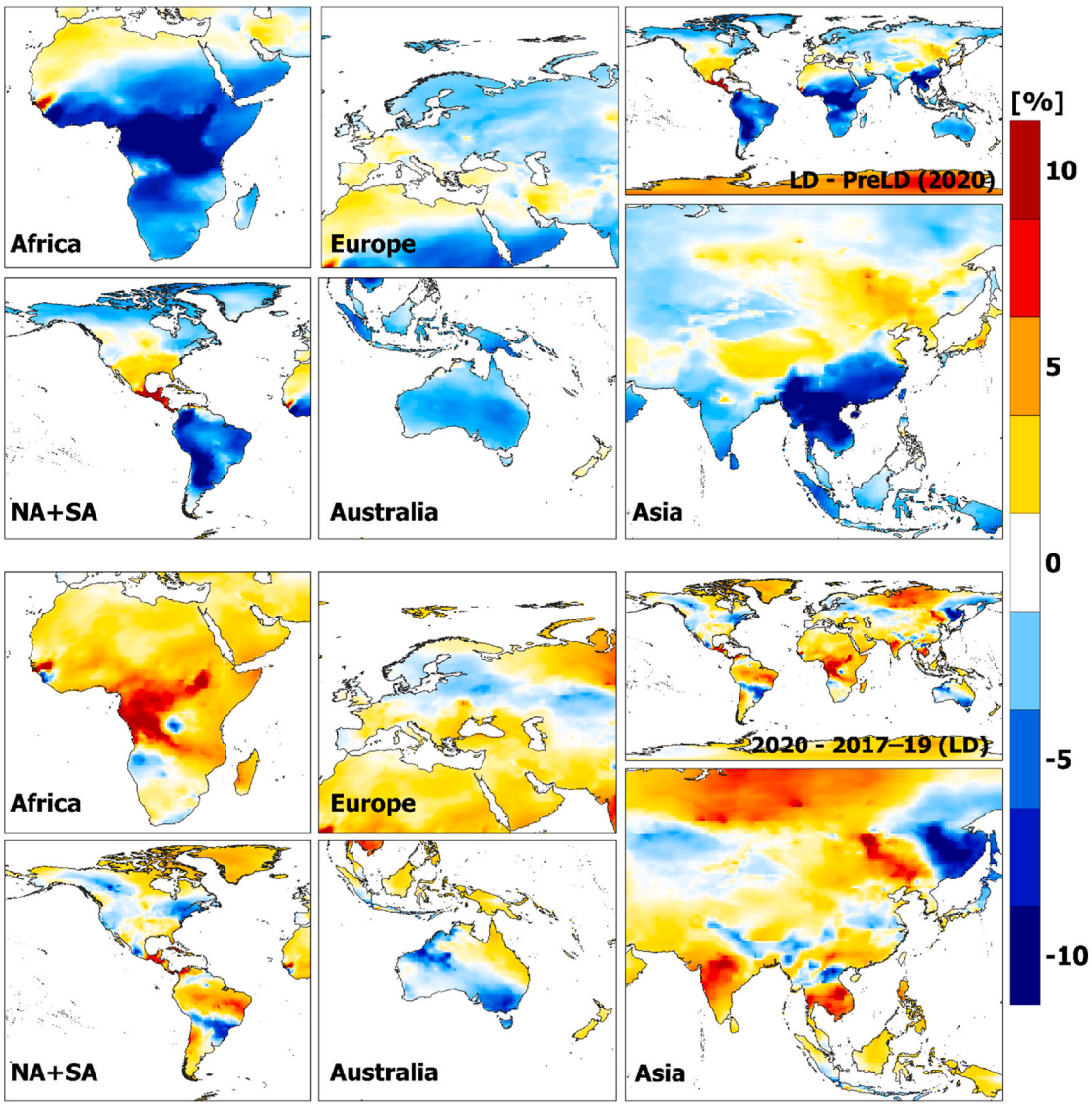

Fig. 2. Changes in the global CO column derived from MERRA–2 during the lockdown (LD: April–May 2020) compared to pre lockdown (PreLD: March 2020) and 2017–2019 average (April–May), where NA is North America and SA is South America.

CO during LD as compared to PreLD, except in the southeastern Russia near China, north USA and Mexico, where an increase of about 2.5–5% is observed in CO. Relatively high reduction is observed in the regions influenced by biomass burning (Figure S2). For example, a reduction of about 5–10% is observed in CA, SA and SEA. The difference in CO between these periods (LD and PreLD) indicates its reduction across the globe, particularly in EC due to shutdown of anthropogenic sources, and in CA, SA and SEA due to the high emissions attributed to the seasonal wildfires and agricultural emissions during PreLD, as inferred from the burnt area in Figure S2. Europe, Australia and India also show a reduction of about 2.5–5% in CO, but have diverse sources such as AWB in India and bush fires in Australia, which were least affected by LD. In addition, the IGP region, where AWB is prevalent during April and May (Kuttippurath et al., 2022), has also experienced a decline in CO emissions. This reduction is due to the decrease in human activities, such as those from industries and vehicles, as a result of LD. The MOPITT CO observations also show similar heterogeneity in different regions across the continents (Figure S3).

3.3. Changes in CO during LD compared to 2017–19 and 2021

The LD impacted anthropogenic sources across the globe, but the reduction in biomass burning regions like CA indicate seasonality in the CO emissions, which can also be confirmed by low CO column and reduced burnt area (>80%) during the LD months (April–May) of 2017–19 (Fig. 2 and Figure S2). The complete LD in India was observed from April to May 2020, followed by a partial PostLD period in few of its states. However, the regions with thermal power plants and refineries show constant CO column throughout the year in India, with a considerable reduction during the PostLD period due to the aforementioned reasons together with the residual impact of shutdown (e.g. Kuttippurath et al., 2023b). The change in CO during LD periods in 2020 and 2017–19 shows a reduction (around 5%) in the regions of high anthropogenic activities (EC, IGP, NA, parts of Europe and Russia), as well as in the areas of frequent wildfires and AWB. In aadition, the reduction in CO column in IGP and central Europe can also be attributed to the reduction in burnt area during this period (Fig. 2 and Figure S2). Similarly, Australia, where the emissions from road transport are very high, shows reduction of 5% in CO column. Similar decline in CO is also observed in Paraguay, and regions of Brazil including Sao Paulo and Parana.

Changes in CO during LD 2020 compared to that of 2021 are illustrated in Figure S4. It is observed that CO was higher in 2020 in India, including IGP, about 5–10%. Similarly, CO was lower in 2021 as

compared to that during LD 2020 after the full resumption of anthropogenic activities in 2021. Both EC and IGP regions are anthropogenically driven with high industrial and AWB activities, and show a decline of about 5–20% in 2021, which can be attributed to the long-term measures like policy implementations and regulations in India (Kuttippurath et al., 2023b) and China clean air policies implemented during 2010–2017 (Zheng et al., 2018) to control air pollution, together with considerable decrease in AWB. The western Europe and eastern USA show a significant rise in CO column in 2021 with respect to 2020, about 5–20%, which is similar its pollution levels in the previous years.

The change in annual mean CO (Fig. 3) column derived from MERRA–2 during 2020 with respect to 2017–19 shows higher values (>10%) in the regions of forest and savannas (CA, Brazil and Russia). However, there is a noticeable decline in CO during the same period in SEA and EC, about −5 to −10%. In 2021, when the restrictions were lifted, the CO amount increased to previous year levels, particularly in NA and Europe, which are the high CO regions dominated by vehicular emissions (Dey and Dhal, 2019; Joshi et al., 2023). It indicates that more stringent environmental laws and vehicular norms are essential to reduce the current pollution levels. On the other hand, there is higher CO during 2020 compared to 2021 in CA, EC, IGP and SA, which can be due to the higher wildfire and AWB in 2020 (Figure S3).

3.4. Regional changes in CO during LD

We examine the changes in average CO column in each country during LD compared to that during PreLD, PostLD, 2017–19 average and 2021, as illustrated in Fig. 4. High heterogeneity in CO change is found in the country scale. For instance, a decline in CO of about 8–25% during LD compared to PreLD is observed in the countries situated in CA such as Congo, Rwanda, Gabon and Nigeria. A comparable reduction in CO is also found in Brazil, Myanmar, Laos, Thailand, Cambodia, Indonesia and Australia. A reduction in CO is also found in the countries, where mixed sources like AWB, vehicular, industrial and residential emissions are dominant [e.g. India (6%), China (2%) and Europe (2%)]. On the other hand, most countries show a slight increase (around 6%) in CO during LD with regard to its 2017–19 average. The CO column in the European and North American countries reached their previous year values during the PostLD period.

We also examine the CO changes in global cities, as the country and regional level analyses alone do not provide local scale changes in CO during LD (Fig. 4). The cities of Central and South India, Laos, Thailand, Cambodia, SA, and particularly CA, have high CO column during the LD months in 2020 compared to the PreLD period, which can be due to the transport of pollutants from nearby regions where biomass burning was prelevant during LD months. However, cities in Canada, Bolivia, Paraguay, Uruguay, Sweden, Norway, IGP, EC and Russia, where anthropogenic activities are the predominant sources of CO, show a significant reduction (around 10%) during LD in 2020 compared to the same months of 2017–19 as a result of tighter restrictions on industrial and vehicular sectors during the former period, consistent with the results of Sokhi et al. (2021), in which they report a decline of up to 30% in CO during LD in cities of aforementioned regions.

The PreLD period shows high CO column in all regions as compared to that in LD, except some cities in Russia, USA, Spain, France, Mexico and China, where they show high CO column during LD. For instance, the primary source of CO in Mexico City is transport associated with gasoline consumption, which produce 95% of all CO (Riveros et al., 1995). However, the CO column rose due to atmospheric transport and dispersion of CO from the nearby region having peak fire season during the LD period. Increase in CO is observed in the cities of China, Russia, USA, Spain and France, where the LD period has higher fire events in the

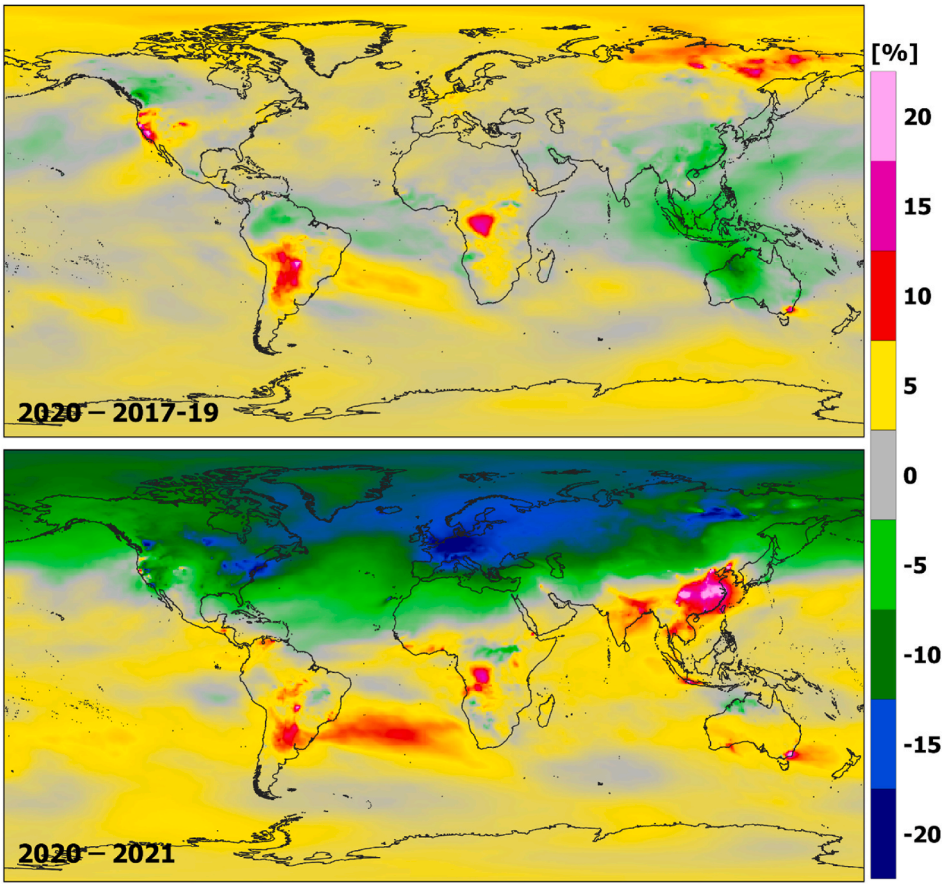

Fig. 3. Changes in the global CO derived from MERRA-2 reanalysis data. The change is calculated based on the annual mean for the corresponding year.

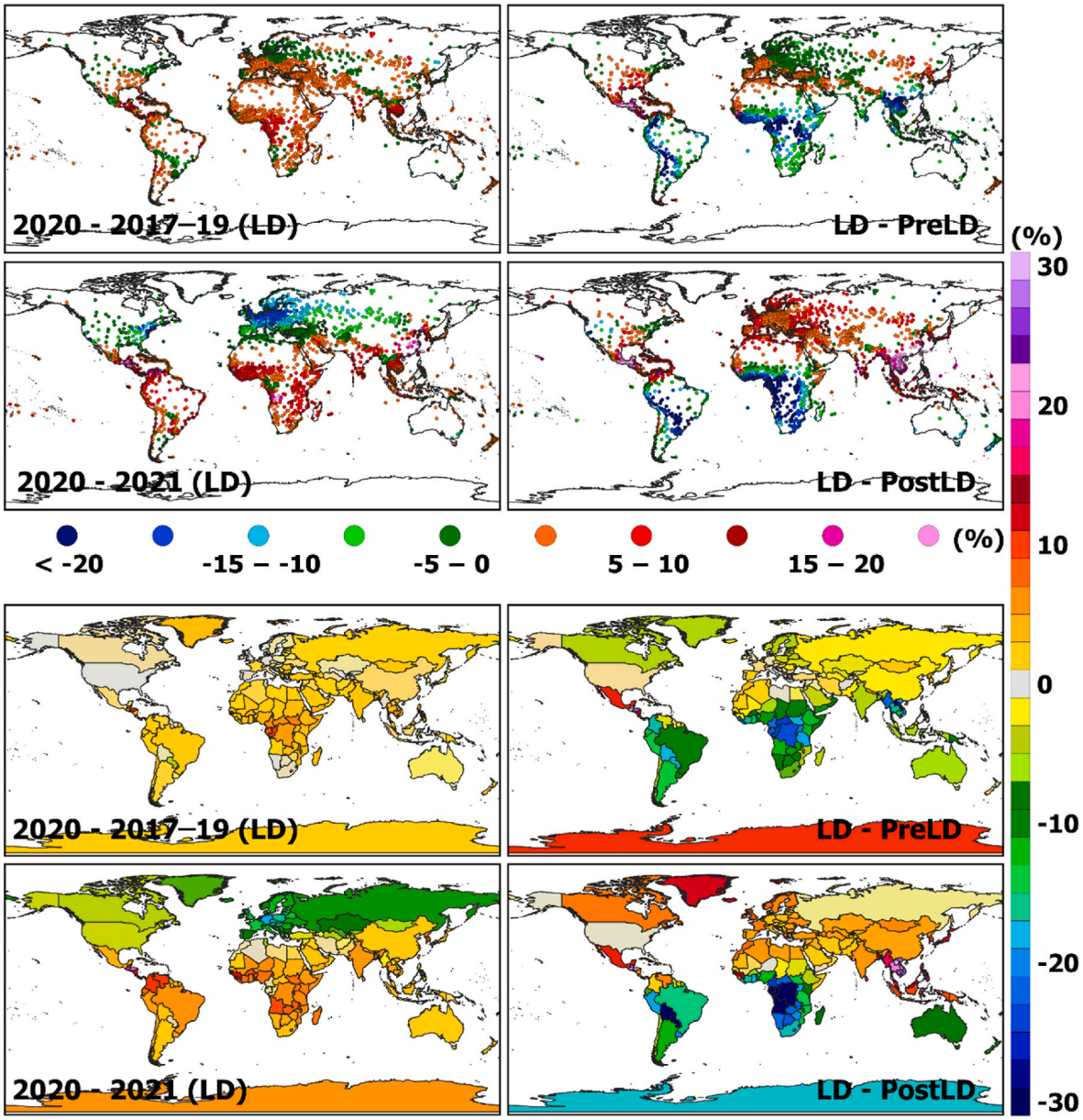

Fig. 4. Top: Change (%) in CO column over the selected global cities (3000 cities with population more than 50000) using the MERRA–2 reanalysis during the lockdown (LD: April–May 2020) compared to pre lockdown (PreLD: March 2020), 2017–2019 (April–May) average and post-lockdown (PostLD: June–September) for the PreLD, LD and PostLD periods. Bottom panel represents the mean change in CO during the same periods in all countries.

nearby agriculture or forest areas as compared to the PreLD period (Global Forest Watch, 2023). The impact of transport of CO emissions from nearby regions might also be responsible for the high CO column in the cities in proximity of intensive fire areas. The resolution of MOPITT is $1^\circ \times 1^\circ$, which is not sufficient to capture the changes in a small region or city, which could also be a reason for the high CO column in the cities during forest fire or AWB events in the nearby areas. However, these changes in CO column are visible in the local scales (e.g. cities in IGP and EC).

The difference in CO during the LD and PostLD months indicates higher CO in the northern hemisphere, which can be attributed to the harvest of seasonal crops (April–May), whereas cities in that region encounter transport of pollutants through nearby rural and agricultural areas (Figure S5). Regions in the southern hemisphere have higher CO during PostLD due to the enhanced heating, use of fossil fuels in austral winters and AWB and wildfires there, although the wildfires impact air quality over large areas in NA, Russia and China (Holloway et al., 2000; Buchholz et al., 2018). High CO column from June to September in the southern hemisphere might also be due to less hydroxyl (OH) concentrations (Novelli et al., 1999), as CO reacts with OH radical to form CO_2, and this reaction is the largest sink of CO and OH in the atmosphere (Lu and Khalil, 1993; Kuttippurath et al., 2023a).

3.5. Changes in tropospheric and stratospheric CO

Several studies have investigated the impact of LD on surface level pollutants, and many of these studies have shown significant reductions in air pollution due to reduced transportation and industrial activities. However, the question of whether these reductions in the air pollution also extend to the tropospheric and stratospheric altitudes is still unanswered. The global and regional changes in CO during COVID–19 LD from near surface to troposphere (1000–100 hPa) and stratosphere (100–1 hPa) using the AIRS measurements are shown in Fig. 5. The difference between CO column during LD and PreLD indicates its global

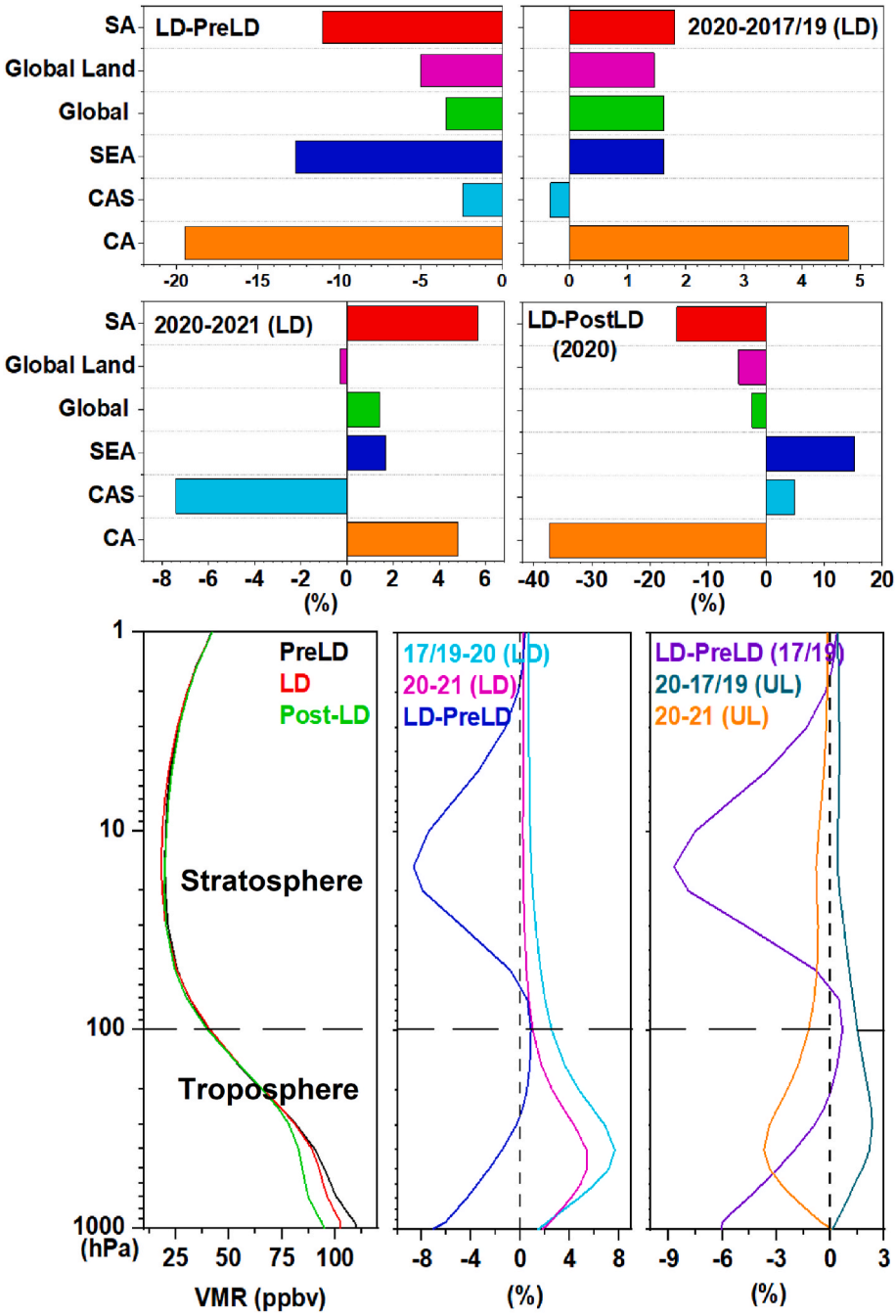

Fig. 5. Top: global and regional changes in CO during lockdown (LD: April–May 2020) compared to pre lockdown (PreLD: March 2020) and post-lockdown (PostLD: June–September) derived from the MERRA–2 reanalysis. Bottom: changes in the volume mixing ratio of CO from near surface to stratosphere derived from the AIRS satellite measurements during the same period. Here: 1000–100 hPa is troposphere and 100–1 hPa is stratosphere.

decrease during LD, but no change is observed in the stratosphere. The difference in CO between the LD months of 2020 and 2017–19 shows its increase, which can be due to the regional change, except in CEA, as illustrated in Fig. 5. The overall effect of LD is the drop in CO by about 0.2% over the land, with the highest reduction in CEA (7%) during LD in 2020 as compared to the same period in 2021. However, with respect to PreLD, there is a high decrease in CO column in LD, with the reduction in CA (19.5%), SEA (12.5%), SA (11%), global average, global land average and CEA (<5%). The PostLD phase in 2020 enhanced the CO column in CA (38%), SA (16%), global land and global average (<5%), except in SEA (−15%) and CEA (−5%). The difference in LD and PostLD CO indicates a decrease in all regions associated with anthropogenic activities (e.g. SA, global land and CA).

When we examine the change in CO column at different altitudes from surface to stratosphere during PreLD, LD and PostLD, it is visible only in the lower troposphere (below 500 hPa). The LD period in 2020 shows lower CO in the troposphere as compared to the same months in 2021. However, no change in stratosphere is found during LD, and this could be due to the transport time needed to get the pollutants to the stratosphere, and the life time of CO at these altitudes. A reduction in CO column is observed in the troposphere during LD in comparison to the same months of 2017–19 together with a minor reduction in the lower stratosphere (<3%). The difference in CO column between LD and PreLD period in 2020 and 2017–19 shows no major change from surface to stratosphere; indicating less impact of LD globally on CO (<3%) at these altitudes. Higher CO column in 2021 than the same period in 2020

indicates the increase in anthropogenic activities after the restrictions were removed, yet there is no change in the stratosphere.

3.6. Role of vehicular, industrial and biomass burning

Fig. 6 and Figure S6 illustrate the NO_2/CO and SO_2/CO ratios during the PreLD, LD and PostLD periods of 2019, 2020 and 2021 using the observations from TROPOMI, respectively. The influence of biogenic emissions on the CO column is examined using the NO_2/CO ratio. Its high values indicate traffic dominated conditions in cities, but small ratios suggest contributions from other sources, such as domestic, agriculture or wildfire events. The contribution of industrial sources in the high CO column is indicated by the high SO_2/CO ratio. We discuss below the changes in the ratios from 2020 to 2019 and then to 2021.

A reduction in NO_2/CO ratio is observed during LD in 2020 compared to the PreLD months in 2020 across all cities, except Sydney, Hamburg, Melbourne and Shanghai (Fig. 6). A clear reduction of CO across all cities in LD 2020 compared to the LD period of 2019 is detected in the analyses. However, enhanced NO_2/CO ratio during 2021 LD months in the cities indicate an increase in the contribution of vehicular emissions towards high CO column. Cities like Rio de Janeiro, Kinshasa, Nairobi, Delhi, Kolkata, Chennai, Bengaluru, Hyderabad, Shanghai, Beijing and Tokyo, where the CO column was high during LD in 2020 as compared to that in 2021, and the NO_2/CO ratio is lower, points out the contribution of transported CO from agriculture, domestic biomass burning or forest fire regions. Higher SO_2/CO ratio (Figure S6) during 2020 LD as compared to that during 2021 LD period in Rio de Janeiro suggests the impact of industrial and power generation sources. Major cities like New York and Moscow show improvements in air quality during LD in 2020, as also illustrated by the NO_2/CO ratio. However, after the restrictions were lifted, the emissions reached PreLD concentrations. A continuous reduction in CO column is observed in Indian and Chinese cities from 2019 to 2021 even with a high NO_2/CO ratio in 2021 and reduced or unchanged SO_2/CO ratio. This suggests the effectiveness of long-term emission control measures in industries and power plants for reducing the overall CO and SO_2 emissions, as also mentioned by Kuttippurath et al. (2022).

In Shanghai, a high NO_2/CO ratio is found during LD 2020; 2021, whereas similar SO_2/CO values with higher CO column in 2020 LD compared to that in 2021 LD period. This enhanced CO column can be attributed to vehicular emissions. The NO_2/CO and SO_2/CO ratios show no change during 2019–2021 PreLD, LD and PostLD periods due to the absence of industrial and vehicular sources in the selected regions of Russia, NA, SA and South Africa. Cities of Moscow, Leeds, London, Munich, Bremen, Washington D.C., Birmingham (US) and New York show reduction in SO_2/CO ratio which might be due to national lockdowns, but no major change in other cities. The changes observed in SO_2/CO ratio require further investigation for individual cities.

3.7. Policy implications for improving air quality

Emissions of CO are generally attributed to anthropogenic activities, AWB and forest fires. The CO emissions from MERRA-2, as shown in Figure S7, indicate that LD reduced the CO emissions as compared to the PreLD period in the hotspots for those few LD months. However, after the restrictions were lifted, the situation became even worse as PostLD shows higher emissions (>18 g/m^2/yr) in the USA and Russia, whereas the high CO in CA and Brazil is due to the seasonal fires there. City

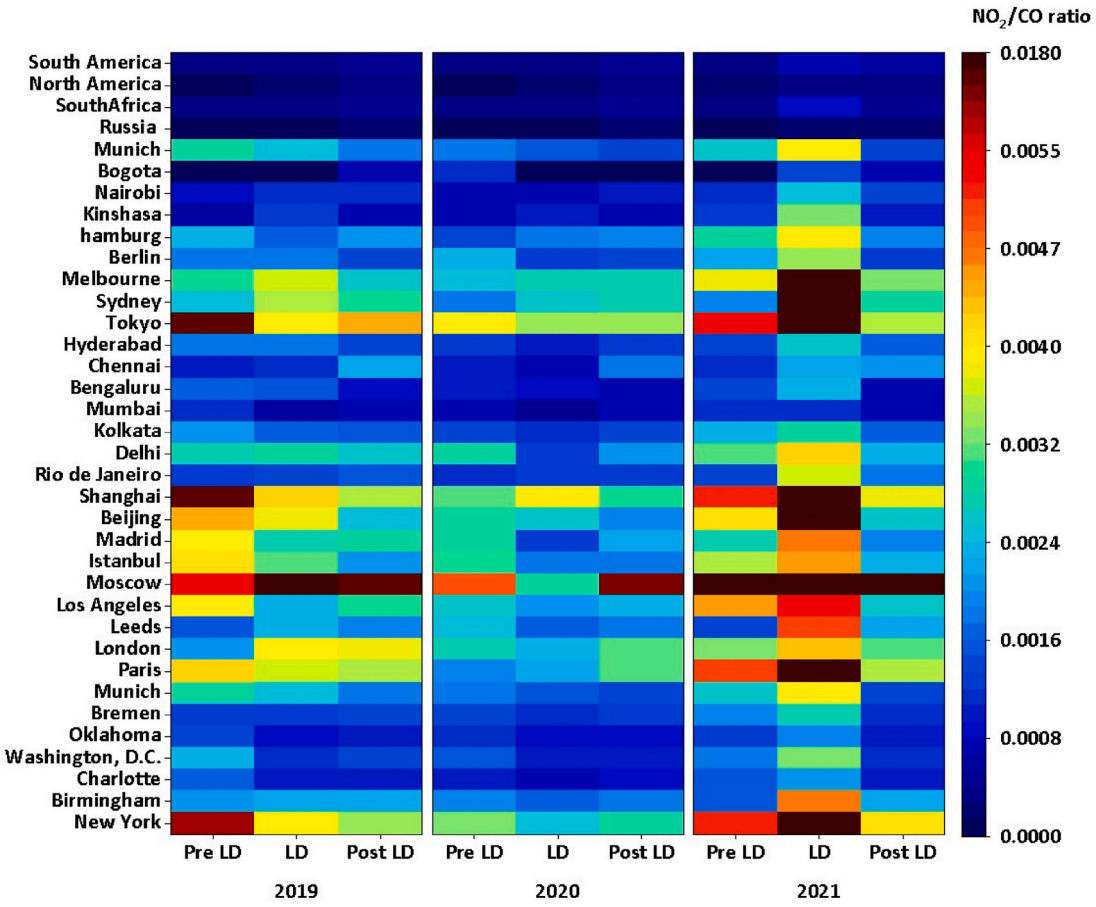

Fig. 6. The NO_2/CO ratio derived using the TROPOMI data from the period 2019–2021 for pre-lockdown (PreLD: March 2020), lockdown (LD: April–May 2020) and post-lockdown (PostLD: June–September) periods over selected regions and cities across the globe.

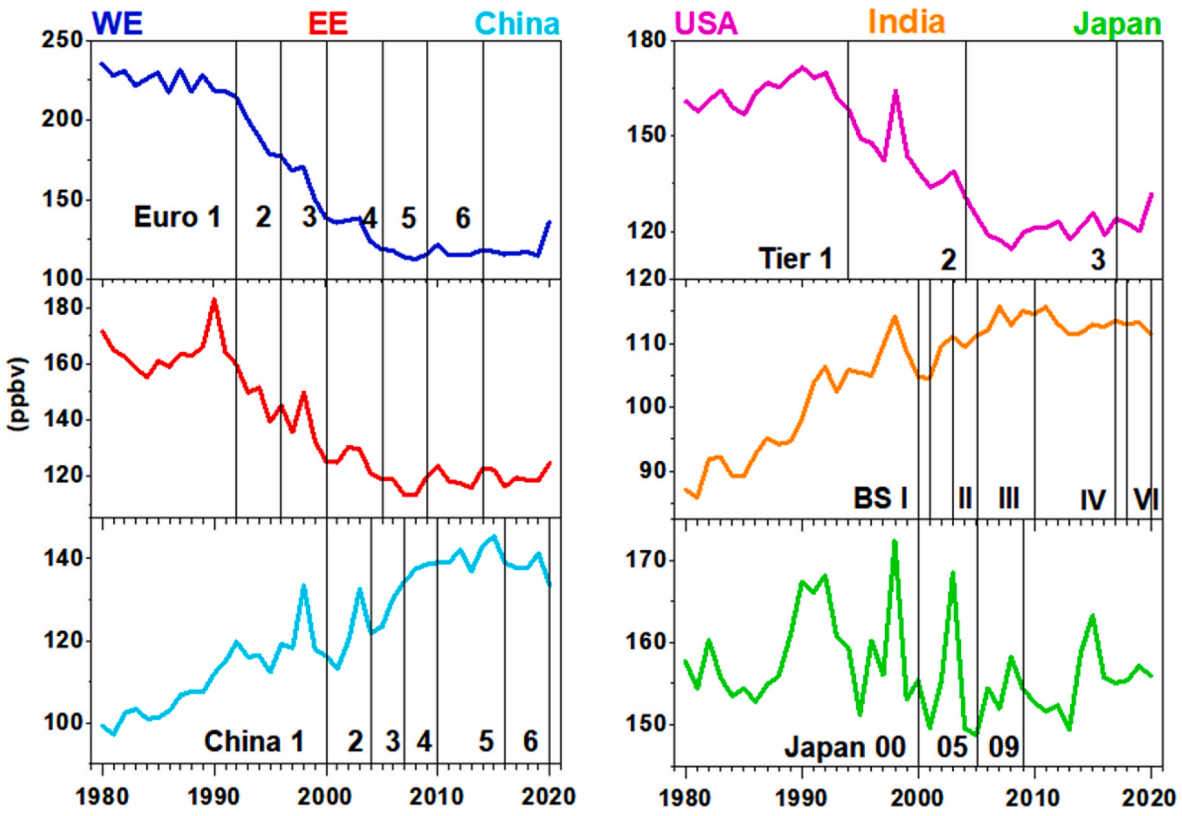

Fig. 7. Changes in CO surface concentration during 1980–2022 derived from the MERRA-2 reanalysis along with the vehicular emission norms implemented in different countries and regions such as the western Europe (WE), eastern Europe (EE), the United States of America (USA), China, India and Japan, where BS is the Bharat Stage vehicular norm.

analysis also indicates that CO reaches its PreLD level after restrictions were eased. Currently there are vehicular emission policies in different countries like USA, China, Europe, Japan and India that help to reduce the air pollution. For example, in the USA, the CO levels declined after the implementation of TIER 1 in 1994 and subsequent tier policies thereafter (Fig. 7). Similarly, in Europe and Japan, the vehicular policies helped to reduce the CO pollution, but it remained constant during the subsequent stages (2005 onwards, after implementation of Euro 4) of the norm implementation. On the other hand, the average CO level in China is gradually increasing even with vehicular norms, which can be due to the dominance of other sources like industries. In India, the CO concentration in the last decade is almost constant during implementation of Bharat Stage II norms (2005 onwards). The CO levels show an increase in PostLD as compared to that during LD. It indicates that more stringent vehicular norms are needed, and environmental policies and novel technologies in different sectors are inevitable to improve the air quality. For instance, significant improvements in air quality have been made since the implementation of regional agreements such as the Convention of Long-Range Transboundary Air Pollution (CLRTAP) of the United Nations Economic Commission for Europe (UNECE) (e.g. vision and strategic priorities set out in the long-term strategy for the Convention for 2020–2030 and beyond, ECE/EB.AIR/142/Add.2, decision 2018/5). In summary, effective policy decisions and their implementations in the local and global scales may contribute to better air quality. In addition, a critical transition is needed towards clean energy, implementation of regulations to reduce agriculture emissions, and well-aligned air quality and climate policies that generate co-benefits across the entire energy sector.

4. Conclusions

Regions associated with anthropogenic emissions from industries and vehicles have shown high reduction in CO concentrations due to LD, but the seasonal AWB, wildfires in forests, grasslands and savannas [CA (−10%), Brazil (−7%), Canada (+3%) and Russia (+3%)] show an increase in the CO column as these were not impacted by LD. Vehicular emissions are the major contributor to CO emissions in the USA and Europe, whereas the AWB, industrial and residential emissions contribute to the high CO levels in India and China. In Amazonia, Indonesia, CA, Russia and SEA, forest fires contribute to the temporal and spatial variability in the atmospheric CO. Cities like Rio de Janeiro, Nairobi, Delhi, Kolkata, Chennai, Bengaluru, Hyderabad, Shanghai, Beijing and Tokyo with high CO column and low NO_2/CO ratio (<0.0016) during 2020 LD as compared to 2021, indicate the contribution of CO transported from agriculture, domestic, biomass burning or forest fire regions. Higher SO_2/CO ratio in Rio de Janeiro indicates the impact of industrial and power generation sources, whereas the cities like New York and Moscow show improvements in air quality during the 2020 LD in terms of CO, with lower NO_2/CO ratio. Reduction in CO column is observed in the troposphere, but no significant change is visible in the stratospheric CO during LD. Although LD can bring the human related activities to a standstill, it is not a go to solution for improving the air quality. Measures related to cleaner use of fuels in industries and replacing AWB with alternative methods, cap and trade or a carbon tax law if implemented at regional or city scale, can be helpful in improving air quality globally.

Credit authors statement

MP: Conceptualization, Methodology, Formal analysis, Visualization, Validation, Software, Writing – original draft. VKP: Conceptualization, Methodology, Formal analysis, Visualization, Validation, Software, review and editing of the original draft. JK: Conceptualization, Methodology, Visualization, Supervision, review and editing of the

original draft.

Declaration of competing interest

The authors declare that they have no known competing financial interests or personal relationships that could have appeared to influence the work reported in this paper.

Data availability

Data will be made available on request.

Acknowledgments

We thank the Director, Indian Institute of Technology Kharagpur (IIT Kgp), and Chairman of CORAL IIT Kgp, for facilitating the study. MP, VKP acknowledge the support from MoE and IIT KGP. We thanks to Google earth engine for maintaining TROPOMI data, Giovanni online data system, developed and maintained by the NASA GES DISC for AIRS, MOPPIT and MERRA 2 data.

Appendix A. Supplementary data

Supplementary data to this article can be found online at https://doi.org/10.1016/j.envpol.2023.122269.

References

Apituley, A., Pedergnana, M., Sneep, M., Veefkind, J.P., Loyola, D., Landgraf, J., Borsdorff, T., 2018. Sentinel-5 Precursor/TROPOMI Level 2 Product User Manual Carbon Monoxide. http://www.tropomi.eu/sites/default/files/files/Sentinel-5P-Level-2-Product-User-Manual Carbon-Monoxide_v1.00.02_20180613.pdf.

Aumann, H.H., Chahine, M.T., Gautier, C., Goldberg, M.D., Kalnay, E., McMillin, L.M., Revercomb, H., Rosenkranz, P.W., Smith, W.L., Staelin, D.H., Strow, L.L., Susskind, J., 2003. AIRS/AMSU/HSB on the Aqua mission: design, science objectives, data products, and processing systems. IEEE Trans. Geosci. Rem. Sens. 41 (2), 253–264. https://doi.org/10.1109/TGRS.2002.808356.

Bhat, S.A., Bashir, O., Bilal, M., Ishaq, A., Dar, M.U.D., Kumar, R., Bhat, R.A., Sher, F., 2021. Impact of COVID-related lockdowns on environmental and climate change scenarios. Environ. Res. 195, 110839 https://doi.org/10.1016/j.envres.2021.110839.

Bray, C.D., Nahas, A., Battye, W.H., Aneja, V.P., 2021. Impact of lockdown during the COVID-19 outbreak on multi-scale air quality. Atmos. Environ. 254, 118386 https://doi.org/10.1016/j.atmosenv.2021.118386.

Buchholz, R.R., Hammerling, D., Worden, H.M., Deeter, M.N., Emmons, L.K., Edwards, D.P., Monks, S.A., 2018. Links between carbon monoxide and climate indices for the southern hemisphere and tropical fire regions. J. Geophys. Res. Atmos. 123 (17), 9786–9800. https://doi.org/10.1029/2018JD028438.

Buchholz, R.R., Deeter, M.N., Worden, H.M., Gille, J., Edwards, D.P., Hannigan, J.W., Jones, N.B., Paton-Walsh, C., Griffith, D.W.T., Smale, D., Robinson, J., Strong, K., Conway, S., Sussmann, R., Hase, F., Blumenstock, T., Mahieu, E., Langerock, B., 2017. Validation of MOPITT carbon monoxide using ground-based Fourier transform infrared spectrometer data from NDACC. Atmos. Meas. Tech. 10, 1927–1956. https://doi.org/10.5194/amt-10-1927-2017.

Chen, Y., Ma, Q., Lin, W., Xu, X., Yao, J., Gao, W., 2020. Measurement report: long-term variations in carbon monoxide at a background station in China's Yangtze River Delta region. Atmos. Chem. Phys. 20 (24), 15969–15982. https://doi.org/10.5194/acp-20-15969-2020.

Dey, S., Dhal, G.C., 2019. Materials progress in the control of CO and CO2 emission at ambient conditions: an overview. Mater. Sci. Energy Technol. 2 (3), 607–623. https://doi.org/10.1016/j.mset.2019.06.004.

El-Sheekh, M.M., Hassan, I.A., 2021. Lockdowns and reduction of economic activities during the COVID-19 pandemic improved air quality in Alexandria, Egypt. Environ. Monit. Assess. 193, 1–7. https://doi.org/10.1007/s10661-020-08780-7.

Filonchyk, M., Hurynovich, V., Yan, H., Gusev, A., Shpilevskaya, N., 2020. Impact assessment of COVID-19 on variations of SO2, NO2, CO and AOD over East China. Aerosol Air Qual. Res. 20 (7), 1530–1540. https://doi.org/10.4209/aaqr.2020.05.0226.

Gelaro, R., McCarty, W., Suárez, M.J., Todling, R., Molod, A., Takacs, L., Randles, C.A., Darmenov, A., Bosilovich, M.G., Reichle, R., Wargan, K., Lawrence, C., Cullather, R., Draper, C., Akella, S., Buchard, V., Conaty, A., da Silva, A.M., Gu, W., Kim, G.K., Koster, R., Lucchesi, R., Merkova, D., Nielsen, J.E., Partyka, G., Pawson, S., Putman, W., Rienecker, M., Schubert, S.D., Siemkiewicz, M., Zhao, B., 2017. The modern-era retrospective analysis for research and applications, version 2 (MERRA-2). J. Clim. 30 (14), 5419–5454. https://doi.org/10.1175/JCLI-D-16-0758.1.

Global Forest Watch, 2023. Fires in Mexico. from. www.globalforestwatch.org. (Accessed 28 January 2023).

Grange, S.K., Lee, J.D., Drysdale, W.S., Lewis, A.C., Hueglin, C., Emmenegger, L., Carslaw, D.C., 2021. COVID-19 lockdowns highlight a risk of increasing ozone pollution in European urban areas. Atmos. Chem. Phys. 21 (5), 4169–4185. https://doi.org/10.5194/acp-21-4169-2021.

Guevara, M., Jorba, O., Soret, A., Petetin, H., Bowdalo, D., Serradell, K., Carles Tena, C., van der Gon, H.D., Kuenen, J., Peuch, V.H., Pérez García-Pando, C., 2021. Time-resolved emission reductions for atmospheric chemistry modelling in Europe during the COVID-19 lockdowns. Atmos. Chem. Phys. 21 (2), 773–797. https://doi.org/10.5194/acp-21-773-2021.

Hammam, E.E., Al Ghamdi, M.A., Almazroui, M., Hassan, I.A., 2022. The COVID-19 pandemic: quantification of temporal variations in air pollutants before, during and post the lockdown in Jeddah city, Saudi Arabia. Earth Syst. Environ. 6 (4), 917–926. https://doi.org/10.1007/s41748-022-00328-8.

Hegarty, J.D., Cady-Pereira, K.E., Payne, V.H., Kulawik, S.S., Worden, J.R., Kantchev, V., Worden, H.M., McKain, K., Pittman, J.V., Commane, R., Daube Jr., B.C., Kort, E.A., 2022. Validation and error estimation of AIRS MUSES CO profiles with HIPPO, ATom, and NOAA GML aircraft observations. Atmos. Meas. Tech. 15, 205–223. https://doi.org/10.5194/amt-15-205-2022.

Holloway, T., Levy, H., Kasibhatla, P., 2000. Global distribution of carbon monoxide. J. Geophys. Res. Atmos. 105 (D10), 12123–12147. https://doi.org/10.1029/1999JD901173.

Joshi, A., Pathak, M., Kuttippurath, J., Patel, V.K., 2023. Adoption of cleaner technologies and reduction in fire events in the hotspots lead to global decline in carbon monoxide. Chemosphere 336, 139259. https://doi.org/10.1016/j.chemosphere.2023.139259.

Khalil, M.A.K., Rasmussen, R.A., 1990. The global cycle of carbon monoxide: trends and mass balance. Chemosphere 20 (1–2), 227–242. https://doi.org/10.1016/0045-6535(90)90098-E.

Krecl, P., Targino, A.C., Oukawa, G.Y., Junior, R.P.C., 2020. Drop in urban air pollution from COVID-19 pandemic: policy implications for the megacity of São Paulo. Environ. Pollut. 265, 114883 https://doi.org/10.1016/j.envpol.2020.114883.

Kuttippurath, J., Ardra, D., Raj, S., Feng, W., 2023a. A seasonal OH minimum region over the Indian Ocean? Atmos. Environ. 295, 119536 https://doi.org/10.1016/j.atmosenv.2022.119536.

Kuttippurath, J., Patel, V.K., Gopikrishnan, G.P., Varikoden, H., 2023b. Changes in air quality, meteorology and energy consumption during the COVID-19 lockdown and unlock periods in India. Air Water Pollut. Rep. 1 (2), 125–138. https://doi.org/10.3390/air1020010.

Kuttippurath, J., Patel, V.K., Pathak, M., Singh, A., 2022. Improvements in SO2 pollution in India: role of technology and environmental regulations. Environ. Sci. Pollut. Res. 29 (52), 78637–78649. https://doi.org/10.1007/s11356-022-21319-2.

Landgraf, J., de Brugh, J.A., Scheepmaker, R., Borsdorff, T., Houweling, S., Hasekamp, O., 2018. Algorithm theoretical baseline document for sentinel-5 precursor: carbon monoxide total column retrieval. Sorbonnelaan 2, 3584. https://sentinel.esa.int/documents/247904/2476257/Sentinel-5P-TROPOMI-ATBD-Carbon-Monoxide-Total-Column-Retrieval.

Lapatinas, A., 2020. The Effect of COVID-19 Confinement Policies on Community Mobility Trends in the EU. Publications Office of the European Union, Luxembourg, p. 5. https://publications.jrc.ec.europa.eu/repository/bitstream/JRC120972/jrc120972_covid_techreport_final.pdf.

Lu, Y., Khalil, M.A.K., 1993. Methane and carbon monoxide in OH chemistry: the effects of feedbacks and reservoirs generated by the reactive products. Chemosphere 26, 641–655. https://doi.org/10.1016/0045-6535(93)90450-J.

Martínez-Alonso, S., Deeter, M., Worden, H., Borsdorff, T., Aben, I., Commane, R., Daube, B., Francis, G., George, M., Landgraf, J., Mao, D., McKain, K., Wofsy, S., 2020. 1.5 years of TROPOMI CO measurements: comparisons to MOPITT and ATom. Atmos. Meas. Tech. 13 (9), 4841–4864. https://doi.org/10.5194/amt-13-4841-2020.

Novelli, P.C., Lang, P.M., Masarie, K.A., Hurst, D.F., Myers, R., Elkins, J.W., 1999. Molecular hydrogen in the troposphere: global distribution and budget. J. Geophys. Res. Atmos. 104 (D23), 30427–30444. https://doi.org/10.1029/92jd00945.

Novelli, P.C., Masarie, K.A., Lang, P.M., 1998. Distributions and recent changes of carbon monoxide in the lower troposphere. J. Geophys. Res. Atmos. 103 (D15), 19015–19033. https://doi.org/10.1029/98JD01366.

Riveros, H.G., Tejeda, J., Ortiz, L., Julián-Sánchez, A., Riveros-Rosas, H., 1995. Hydrocarbons and carbon monoxide in the atmosphere of Mexico City. J. Air Waste Manag. Assoc. 45 (12), 973–980. https://doi.org/10.1080/10473289.1995.10467429.

Said, S., Salah, Z., Abdelmageid Hassan, I., Abdel Wahab, M.M., 2022. COVID-19 lockdown: impact on PM 10 and PM 2.5 in six megacities in the world assessed using NASA's MERRA-2 reanalysis. Asian J. Atmos. Environ. 16 (2), 93–105. https://doi.org/10.5572/ajae.2021.146.

Shi, Z., Song, C., Liu, B., Lu, G., Xu, J., Van Vu, T., Elliott, R.J.R., Li, W., Bloss, W.J., Harrison, R.M., 2021. Abrupt but smaller than expected changes in surface air quality attributable to COVID-19 lockdowns. Sci. Adv. 7 (3), eabd6696. https://www.science.org/doi/10.1126/sciadv.abd6696.

Singh, V., Singh, S., Biswal, A., Kesarkar, A.P., Mor, S., Ravindra, K., 2020. Diurnal and temporal changes in air pollution during COVID-19 strict lockdown over different regions of India. Environ. Pollut. 266, 115368 https://doi.org/10.1016/j.envpol.2020.115368.

Sokhi, R.S., Singh, V., Querol, X., Finardi, S., Targino, A.C., de Fatima Andrade, M., Pavlovic, R., Garland, R.M., Massagué, J., Kong, S., Baklanov, A., Ren, L., Tarasova, O., Carmichael, G., Peuch, V.H., Anand, V., Arbilla, G., Badali, K., Beig, G., Belalcazar, L.C., coauthors, 2021. A global observational analysis to understand

changes in air quality during exceptionally low anthropogenic emission conditions. Environ. Int. 157, 106818 https://doi.org/10.1016/j.envint.2021.106818.
World Health Organization (WHO, 2022). https://www.who.int/news-room/fact-sheets/detail/ambient-(outdoor)-air-quality-and-health.
Zheng, B., Chevallier, F., Yin, Y., Ciais, P., Fortems-Cheiney, A., Deeter, M.N., Parker, R. J., Wang, Y., Worden, H.M., Zhao, Y., 2019. Global atmospheric carbon monoxide budget 2000–2017 inferred from multi-species atmospheric inversions. Earth Syst. Sci. Data 11 (3), 1411–1436. https://doi.org/10.5194/essd-11-1411-2019.
Zheng, B., Tong, D., Li, M., Liu, F., Hong, C., Geng, G., Li, H., Li, X., Peng, L., Qi, J., Yan, L., Zhang, Y., Zhao, H., Zheng, Y., He, K., Zhang, Q., 2018. Trends in China's anthropogenic emissions since 2010 as the consequence of clean air actions. Atmos. Chem. Phys. 18 (19), 14095–14111. https://doi.org/10.5194/acp-18-14095-2018.